PAPER

Check for updates

Dynamical disorder and resonance energy transfer: a novel quantum-classical approach†

F. Di Maiolo [iD] ‡ and A. Painelli [iD] *

Resonance energy transfer (RET), at the heart of photosynthesis, supports life on earth, but also guarantees the operation of several technological devices, like organic light-emitting diodes and solar cells. Medium properties and dynamics largely affect RET efficiency, but reliable models addressing how molecular electron-vibration motion and solvent dynamics jointly affect RET are still missing. Here we propose a novel quantum-classical approach to describe RET in a non-adiabatic molecular system embedded in a dynamic polar environment. The approach, validated against optical properties of a dye in solution, is then applied to a RET-pair, demonstrating that dynamic disorder, as induced by a liquid polar solvent, boosts RET efficiency.

1 Introduction

RET describes the transfer of energy from an excited molecule, the energy donor, to an acceptor molecule, in a process $\mathscr{D}^*\mathscr{A} \to \mathscr{D}\mathscr{A}^*$, where the star marks the excited molecular species. RET, occurring *via* the exchange of a virtual photon,[1] governs energy-transfer processes for intermolecular distances in the 10–100 Å range, where the orbital overlap is negligible and radiative energy transfer can be excluded. The first RET model dates back to 1948,[2] but in spite of continued research in the field, many issues remain unsolved: molecular vibrations,[3] static[4,5] and dynamic[3,6–9] disorder enter the picture. Moreover RET is a dissipative phenomenon and dynamical models for RET require the techniques of open quantum systems. Here, we propose an original dynamical approach to RET where the RET-pair is described by a minimal model that accounts for non-adiabatic electron-vibration coupling. The RET-pair dissipates energy to a Redfield bath $\mathscr{B}_1$,[10] that accounts for the coupling between the system and fast environmental degrees of freedom and hence accounts for homogeneous broadening (fast disorder). Moreover the system is coupled to a pair of overdamped (classical) oscillators $\mathscr{B}_2$,[11] mimicking polar solvation, an effective source of inhomogeneous broadening (slow disorder).[12–15] A novel multi-state Redfield–Smoluchowski equation is introduced to study the coupled dynamics of the resulting open quantum-classical system. The proposed approach represents a powerful strategy to address photoexcited state dynamics in the presence of dynamic disorder. The method is first validated addressing the dynamics of a single molecule in solution, following impulsive photoexcitation. Calculated absorption and time-resolved fluorescence spectra demonstrate that the method accounts not just for solvatochromic shifts and for their temporal evolution, but also for homogeneous and inhomogeneous broadening phenomena. In a more ambitious effort, the dynamics of a RET pair is investigated in the same scheme, highlighting the important role of dynamic disorder in speeding up RET processes.

2 The molecular model

The simplest accurate model for optical spectra of organic molecules in solution applies to polar conjugated dyes, whose low-energy physics is governed by the resonance between a neutral state $|N\rangle$, with negligible polarity, and a charge-separated (zwitterionic) state $|Z\rangle$, with a sizable dipole moment μ_0, as shown in Fig. 1a, for two representative dyes, DCM and NR. Essential state models describe the electronic structure of the dye in terms of the corresponding two diabatic states, separated by an energy gap $2z$. Electron-vibration coupling is described introducing a single effective coordinate $\hat{Q}$ that linearly modulates the energy gap, as to account for the different equilibrium geometries associated with $|N\rangle$ and $|Z\rangle$. Introducing the vibrational creation (annihilation) operator $\hat{d}^\dagger$ ($\hat{d}$), the coordinate is $\hat{Q} = \left(\hat{d}^\dagger + \hat{d}\right)\big/\sqrt{2}$, and the molecular Hamiltonian reads:[16]

$$\hat{H}^{\mathrm{mol}} = -\tau\hat{\sigma}_x + 2z\hat{\rho} - \sqrt{\hbar\omega_\mathrm{v}\varepsilon_\mathrm{v}}\,\hat{\rho}\left(\hat{d}^\dagger + \hat{d}\right) + \hbar\omega_\mathrm{v}\left(\hat{d}^\dagger\hat{d} + \frac{1}{2}\right),$$

(1)

Department of Chemistry, Life Science and Environmental Sustainability, Università di Parma, 43124 Parma, Italy. E-mail: anna.painelli@unipr.it

† Electronic supplementary information (ESI) available: Computational details; steady-state optical spectra; complete expressions of the Redfield tensor terms; derivation of eqn (3); equation of motion relevant to the RET-pair; energy donor-energy acceptor gap; video of the RET dynamics in glassy CHCl₃ and in liquid CHCl₃. See DOI: 10.1039/c9cp06038c

‡ Present address: Institute of Physical and Theoretical Chemistry, Goethe University, Frankfurt, Max-von-Laue-Str. 7, 60438 Frankfurt, Germany.
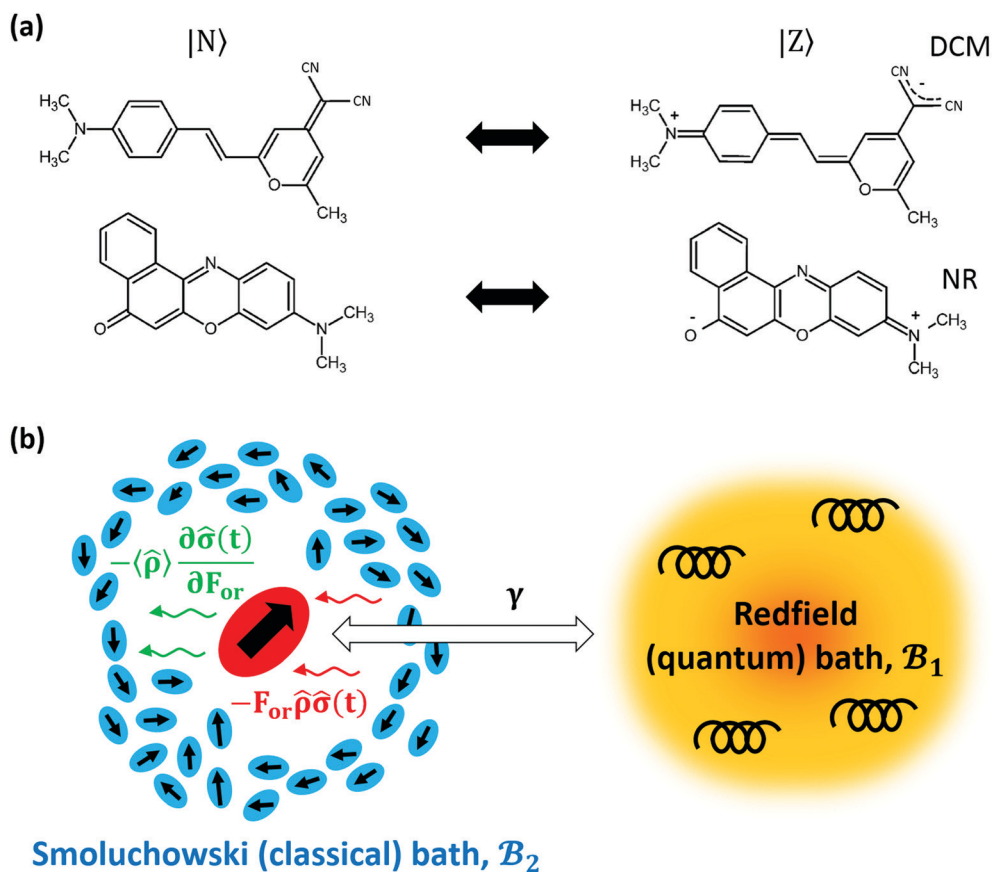
This journal is © the Owner Societies 2020

Phys. Chem. Chem. Phys., 2020, **22**, 1061–1068 | **1061**

Fig. 1 (a) The chemical structure of two polar dyes: (4-(dicyanomethylene)-2-methyl-6-(4-dimethylamino-styryl)-4H-pyran) (DCM) and 9-diethylamino-5-benzo[α]phenoxazinone (Nile-Red, NR). For both dyes the neutral (N) and zwitterionic (Z) resonance structures are shown. (b) Pictorial representation of the different terms entering the multistate Redfield–Smoluchowski equation (*cf.* eqn (3)).

where $\hat{\sigma}_x = |N\rangle\langle Z| + |Z\rangle\langle N|$, $\hat{\rho} = |Z\rangle\langle Z|$ and ω_v and ε_v are the vibrational frequency and relaxation energy, respectively. Numerically exact non-adiabatic eigenstates and eigenvalues ($|\psi_a\rangle$ and E_a, respectively) for the molecular system are obtained upon numerical diagonalization of $\hat{H}^{mol}$ (see ESI†).[15,17]

The model in eqn (1) accounts for the molecular polarity and polarizability and has been successfully extended to describe environmental and solvent effects on optical spectra of polar dyes.[12,13,17] A molecule in solution feels the electric field (the so-called reaction field) generated by the solvent in response to the solute polarity. The fast component of the reaction field is associated with the electronic degrees of freedom of the solvent, as described by its refractive index, and can be treated in the antiadiabatic approximation. This leads to a renormalization of model parameters that, in view of the marginal variability of the refractive index of common organic solvents, are considered solvent independent.[12]

In polar solvents, a slow component of the reaction field F_{or} appears due to the orientational motion of polar solvent molecules around the solute. F_{or} enters the Hamiltonian with a term $-\hat{\rho}F_{or}$, where the prefactor μ_0, in the definition of the dipole moment operator $\hat{\mu} = \mu_0\hat{\rho}$, is included into F_{or} that then acquires energy dimension. If the solvent is treated as an elastic medium, the potential energy is $F_{or}^2/4\varepsilon_{or}$, where ε_{or} is the solvent

relaxation energy, a quantity that measures the solvent polarity.[12] The F_{or}-dependent molecular Hamiltonian can be diagonalized for different F_{or} values and linear and non-linear optical spectra of polar dyes have been successfully calculated[13–15,17] (see ESI†) in an approach that however does not account for relaxation phenomena.

3 The multistate Redfield–Smoluchowski quantum-classical equation

To set up a dissipative model, we follow ref. 18 and couple our system $\mathcal{S}$, described by $\hat{H}^{mol}$, to a Redfield bath $\mathcal{B}_1$, accounting for fast environmental degrees of freedom. $\mathcal{B}_1$ is modeled as a collection of quantum harmonic oscillators $\hat{H}_{\mathcal{B}_1} = \sum_i \hbar\omega_i\left(\hat{b}_i^\dagger\hat{b}_i + 1/2\right)$, where ω_i is the frequency of the i-th oscillator, $\hat{b}_i$ $\left(\hat{b}_i^\dagger\right)$ annihilates (creates) the corresponding quantum. The system-bath coupling is bilinear

$$\hat{H}_{\mathcal{S}\mathcal{B}_1} = \sum_i g_i\left(\hat{b}_i^\dagger\hat{d} + \hat{b}_i\hat{d}^\dagger\right) \tag{2}$$

and describes the exchange of energy quanta between $\mathscr{S}$ and $\mathscr{B}_1$. In line with the fast nature of $\mathscr{B}_1$, the bath spectral density is set equal to the constant term $\hbar^2\gamma/\pi$, where γ has the dimension of frequency.[18,19] The full expression for the Redfield tensor is reported in the ESI.†

The orientational reaction field F_{or} represents a slow variable and is treated as a classical bath, $\mathscr{B}_2$. A hybrid quantum-classical density operator $\hat{\sigma}(F_{or};t)$ is therefore introduced, corresponding to the usual reduced density matrix of the system, written on the basis of $|\psi_a\rangle$ states, *i.e.* on the basis of the non-adiabatic eigenstates of $\hat{H}^{mol}$ in eqn (1). However, to account for polar solvation, the matrix elements of the density matrix acquire a dependence on F_{or}.[20,21] The density matrix is normalized, $\mathrm{Tr}_{\mathscr{S}}\left[\int dF_{or}\hat{\sigma}(F_{or};t)\right] = 1$, and the expectation value of a generic operator $\hat{O}$ is $\langle\hat{O}(t)\rangle = \mathrm{Tr}_{\mathscr{S}}\left[\int dF_{or}\hat{O}\hat{\sigma}(F_{or};t)\right]$, where $\mathrm{Tr}_{\mathscr{S}}[\cdot]$ is the trace over the system degrees of freedom.[22]

The dynamical equation for the hybrid density operator reads (full derivation in ESI†):

$$\frac{\partial}{\partial t}\sigma_{ab}(F_{or};t) = -i\omega_{ab}\sigma_{ab}(F_{or};t) + \sum_{c,d}R_{ab,cd}\sigma_{cd}(F_{or};t)$$

$$+ \frac{-F_{or}}{i\hbar}\sum_c\left(\rho_{ac}\sigma_{cb}(F_{or};t) - \sigma_{ac}(F_{or};t)\rho_{cb}\right)$$

$$- \frac{2\varepsilon_{or}}{\tau_l}\langle\hat{\rho}(F_{or};t)\rangle\frac{\partial\sigma_{ab}(F_{or};t)}{\partial F_{or}}$$

$$+ \frac{1}{\tau_l}\frac{\partial}{\partial F_{or}}\left(F_{or}\sigma_{ab}(F_{or};t) + k_B T 2\varepsilon_{or}\frac{\partial}{\partial F_{or}}\sigma_{ab}(F_{or};t)\right),$$

$$(3)$$

where $\sigma_{ab}(F_{or};t) = \langle\psi_a|\hat{\sigma}(F_{or};t)|\psi_b\rangle$, $\forall a, b = 1,\ldots,N$, and the sums run on $\hat{H}^{mol}$ non-adiabatic eigenstates. The first term in the

above equation describes the Liouvillian dynamics, with $\omega_{ab} = (E_a - E_b)/\hbar$. The second term accounts for the dissipation towards $\mathscr{B}_1$, with $R_{ab,cd}$ representing an element of the Redfield tensor (see ESI†). The third and fourth terms describe the effect of $\mathscr{B}_2$ on the $\mathscr{S}$ dynamics and the $\mathscr{S}$ to $\mathscr{B}_2$ backreaction, respectively (see Fig. 1b). Finally, the last term describes the solvent drift-diffusion Smoluchowski dynamics,[11,15,23] τ_l being the longitudinal relaxation time of the solvent,[24] T the temperature and k_B the Boltzmann constant. The expectation value at the fourth term in eqn (3) is calculated as $\langle\hat{\rho}(F_{or};t)\rangle = \mathrm{Tr}_{\mathscr{S}}[\hat{\rho}\hat{\sigma}(F_{or};t)]$.

4 Dynamics and optical spectra of a solvated organic dye

We are now in the position to calculate the dynamics of a photoexcited molecule in solution starting from an initial ($t = 0$) state with disentangled $\mathscr{S}$ and $\mathscr{B}_2$, *i.e.* $\hat{\sigma}(F_{or};t = 0) = \hat{\sigma} \otimes w(F_{or})$. A coherent (ultrafast) vertical excitation is considered, with $\hat{\sigma}(t = 0) = |\Psi^*\rangle\langle\Psi^*|$, where $|\Psi^*\rangle = \sum_{a=2}^{N}|\psi_a\rangle\langle\psi_a|\hat{\mu}|\psi_1\rangle$. In line with the hypothesis of an ultrafast excitation, the initial solvent distribution is set to the ground state equilibrium $w(F_{or};t = 0) = \exp[-E_1(F_{or})/k_B T]$, where $E_1(F_{or})$ is the F_{or}-dependent ground state energy (see ESI†).

Fig. 2 summarizes results obtained for the DCM dye (molecular parameters in Table 1) dissolved in CHCl₃ ($\varepsilon_{or} = 0.32$ eV,[15] $\tau_l = 2.8$ ps[24]). Computational details can be found in the ESI.† The trajectory in panel (a) shows the evolution of the system energy $\langle\hat{H}^{mol}\rangle$ *vs.* the expectation values of F_{or} and $\hat{Q}$, while the color maps show (for reference purposes) the adiabatic Potential
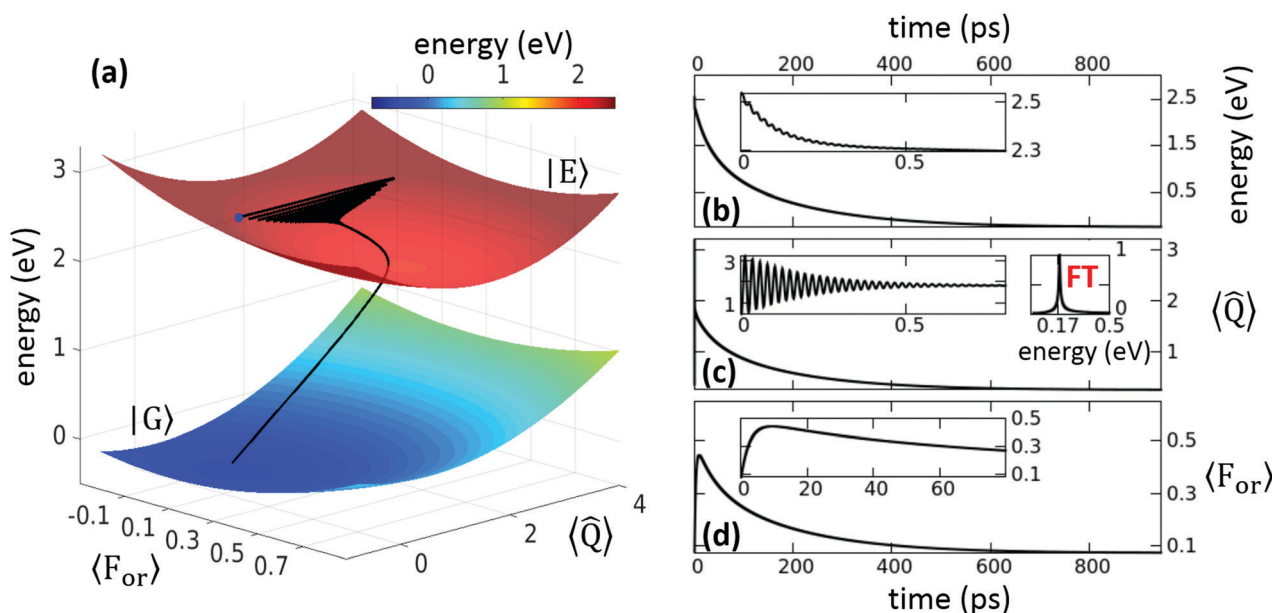

Fig. 2 Room temperature dynamics of coherently excited DCM dye (molecular parameters in Table 1, $\gamma = 5$ ps^{-1}) in liquid CHCl₃ ($\varepsilon_{or} = 0.32$ eV, $\tau_l = 2.8$ ps). (a) Evolution of the $\langle H^{mol}\rangle$ energy *vs.* the expectation values of the vibrational coordinate and of the solvation field. The blue dot represents the starting point of the dynamics. The adiabatic PES are shown for reference. Panels (b), (c) and (d) show the time-dependence of $\langle H^{mol}\rangle$, of the vibrational coordinate, and of the solvation field, respectively. Insets zoom on the early dynamics. An additional inset in panel (c) shows the $\langle\hat{Q}(t)\rangle$ Fourier transform.

Table 1 Model parameters for DCM[15] and NR[25] dyes. All the quantities are in eV

	$2z$	$-\tau$	ε_v	$\hbar\omega_v$
DCM	2.28	0.88	0.456	0.172
NR	1.76	0.95	0.33	0.14

Energy Surfaces (PES) relevant to the ground and excited states. After the initial ultrafast excitation, the system undergoes coherent oscillations before equilibrating towards the minimum of the excited state PES, from where it finally slowly reaches the ground state equilibrium. Fig. 2 also shows the time-evolution of the system energy, and of the expectation values of $\hat{Q}$ and F_{or}. The initial coherent oscillations, observed at frequency slightly larger than ω_v, due to hardening effects in the excited state, extinguish within the first ~ 500 fs, and in about 10 ps the solvent equilibrates towards the minimum of

the excited state PES. Subsequent relaxation towards the ground state is completed in about 0.5 ns (see ESI† for more details).

Absorption spectra of the solvated dye are calculated as the real part of the Fourier transform of the dipole–dipole correlation function $C^a_{\mu\mu}(t) = \langle \hat{\mu}(t)\hat{\mu} \rangle = \mathrm{Tr}_{\mathscr{S}}\left[\int dF_{or}\hat{\mu}\hat{\Omega}^a(F_{or};t)\right]$, where $\Omega^a(F_{or};t)$ is the spectral generating function.[27] At the initial time, the generating function is set to $\hat{\Omega}^a(F_{or};0) = \hat{\mu}|\psi_1\rangle\langle\psi_1| \otimes \exp[-E_1(F_{or})/k_BT]$, where $|\psi_1\rangle$ is the lowest eigenstate of $\hat{H}^{mol}$. Its subsequent dynamics is governed by the same equation governing the density matrix dynamics, eqn (3).[27] Results in Fig. 3 reproduce the inhomogeneous broadening due to polar solvation as well as the progressive red-shift of the absorption band with increasing solvent polarity. On the other hand, accounting for a single effective coupled mode, the proposed model gives rise to a single
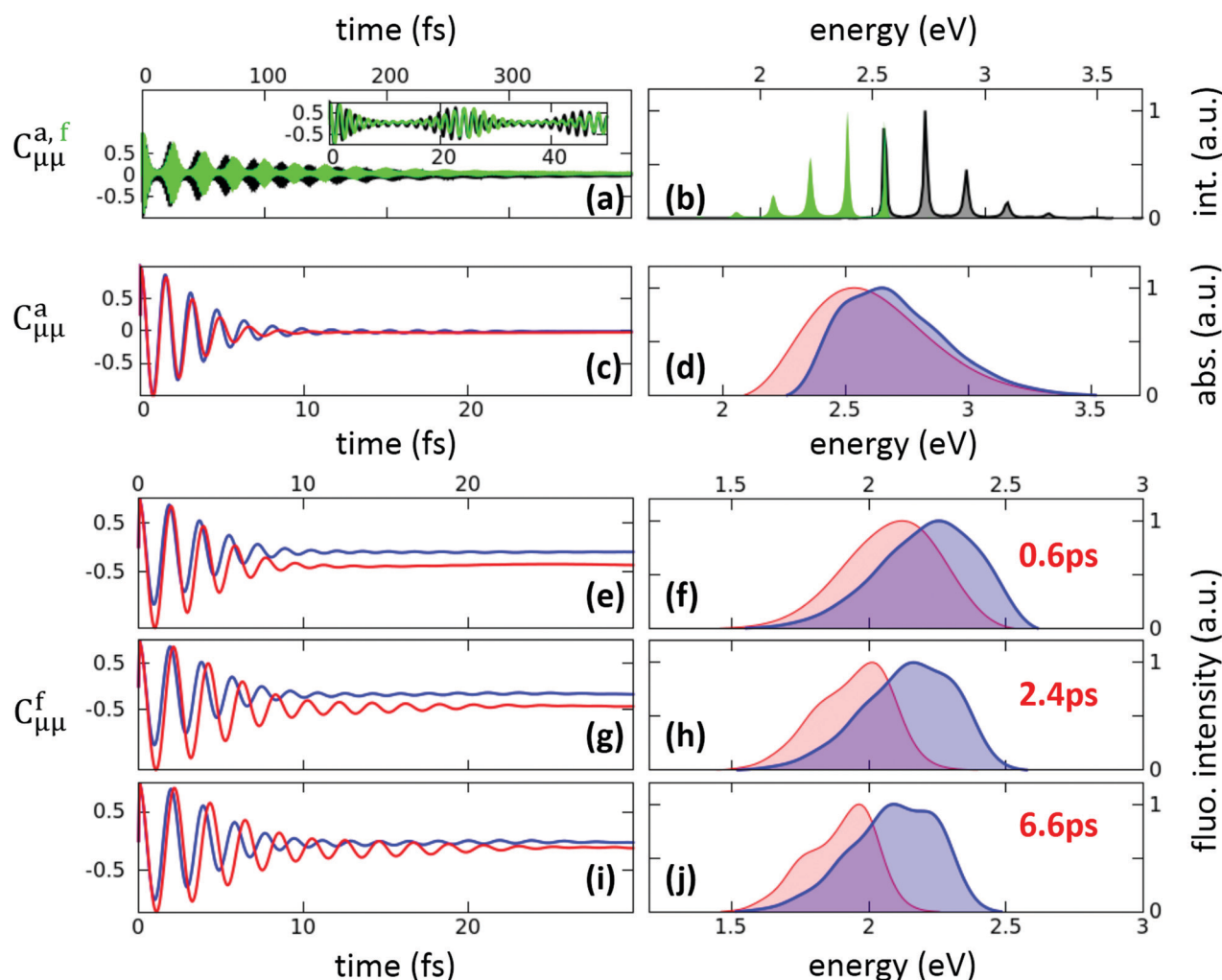

Fig. 3 Calculation of absorption and time-resolved fluorescence spectra of DCM. (a) Time-dependence of $C^a_{\mu\mu}$ (black curve) and $C^f_{\mu\mu}$ (green curve) calculated in a non-polar solvent (cyclohexane, $\varepsilon_{or} = 0$).[15] The inset zooms on the early time; (b) real part of the Fourier transforms of the signals in panel (a). (c) Time-dependence of $C^a_{\mu\mu}$ in CHCl$_3$ (blue curve, same parameters as in Fig. 2) and DMSO ($\varepsilon_{or} = 0.75$ eV,[15] $\tau_l = 2$ ps,[26] red curve); (d) real part of the Fourier transforms of the signals in panel (c). (e, g and i) Time-dependence of $C^f_{\mu\mu}$ in CHCl$_3$ (blue curve) and DMSO (red curve) calculated for different t'; (f, h and j) real part of the Fourier transforms of the signals in panels (e), (g), (i), respectively.

1064 | *Phys. Chem. Chem. Phys.*, 2020, **22**, 1061–1068

This journal is © the Owner Societies 2020

vibronic progression that, in experimental systems, is blurred due to the presence of several coupled modes.

To address time-resolved fluorescence spectra, we coherently excite the ground state and calculate the dynamics of the photoexcited system as described in the previous section. After a time interval t', we define the fluorescence generating function $\hat{\Omega}^{\mathrm{f}}(F_{\mathrm{or}}; t - t', t')$ whose dynamics again obeys eqn (3). For each t', the initial $(t = t')$ generating function is set as $\hat{\mu}\hat{\sigma}(F_{\mathrm{or}}; t')$ and the fluorescence spectrum is calculated as the real part of the Fourier transform of the time correlation function

$$C^{\mathrm{f}}_{\mu\mu}(t - t', t') = \langle\hat{\mu}(t - t')\hat{\mu}(t')\rangle = \mathrm{Tr}_{\mathscr{S}}\left[\int\mathrm{d}F_{\mathrm{or}}\hat{\mu}\hat{\Omega}^{\mathrm{f}}(F_{\mathrm{or}}; t - t', t')\right].$$

Results for different solvents are reported in Fig. 3. The time-evolution of the Stokes shift and of the bandshapes compares favourably with experimental results[14,28,29] and is in line with steady state fluorescence spectra, calculated based on the equilibrated Boltzmann distribution (see ESI†).[30]

5 RET in polar solvent: the role of dynamical disorder

Having validated the proposed approach on optical spectra of a solvated dye, we can now move to RET. Our RET-pair is formed by the two polar molecules shown in Fig. 1a, where DCM acts as the energy donor $\mathscr{D}$, and NR as the energy acceptor $\mathscr{A}$. Both dyes are described by the molecular Hamiltonian in eqn (1) and the RET-pair Hamiltonian reads:

$$\begin{aligned}
\hat{H}^{\mathrm{RET}} &= -\tau_{\mathscr{D}}\hat{\sigma}_{\mathscr{D}} - \tau_{\mathscr{A}}\hat{\sigma}_{\mathscr{A}} + 2z_{\mathscr{D}}\hat{\rho}_{\mathscr{D}} + 2z_{\mathscr{A}}\hat{\rho}_{\mathscr{A}} + V\hat{\rho}_{\mathscr{D}}\hat{\rho}_{\mathscr{D}} \\
&\quad - \sqrt{\hbar\omega_{\mathrm{v}}^{\mathscr{D}}2\varepsilon_{\mathscr{D}}}\hat{\rho}_{\mathscr{D}}\hat{Q}_{\mathscr{D}} - \sqrt{\hbar\omega_{\mathrm{v}}^{\mathscr{A}}2\varepsilon_{\mathscr{A}}}\hat{\rho}_{\mathscr{A}}\hat{Q}_{\mathscr{A}} \\
&\quad + \frac{\hbar\omega_{\mathrm{v}}^{\mathscr{D}}}{2}(\hat{Q}_{\mathscr{D}}{}^2 + \hat{P}_{\mathscr{D}}{}^2) + \frac{\hbar\omega_{\mathrm{v}}^{\mathscr{A}}}{2}(\hat{Q}_{\mathscr{A}}{}^2 + \hat{P}_{\mathscr{A}}{}^2),
\end{aligned} \quad (4)$$

where $\mathscr{D}$ and $\mathscr{A}$ labels specify parameters and operators relevant to the two molecular species. The V-term in the first line of the above equation accounts for the intermolecular electrostatic interaction between the two dyes in the zwitterionic state. As discussed in ref. 18 and 31, this intermolecular interaction drives RET and indeed the above Hamiltonian collapses in the standard Förster model, with interacting transition dipole moments, if the basis is rotated from the diabatic N and Z states to the adiabatic ground and excited states for each molecule.

Following ref. 18, to account for fast environmental degrees of freedom, $\mathscr{D}$ and $\mathscr{A}$ are coupled to a Redfield bath $\mathscr{B}_1$ with constant spectral density $\mathscr{J} = \hbar^2\gamma/\pi$ (see ESI†). For polar solvation we must account for the two reaction fields, $F_{\mathscr{D}}^{\mathrm{or}}$ and $F_{\mathscr{A}}^{\mathrm{or}}$, generated by the solvent in response to the $\mathscr{D}$ and $\mathscr{A}$ dipoles, respectively. The hybrid quantum-classical density operator $\hat{\sigma}(F_{\mathscr{D}}^{\mathrm{or}}, F_{\mathscr{A}}^{\mathrm{or}}; t)$ is therefore defined on a two-dimensional grid and the expectation value of a generic operator $\hat{O}$ is calculated as $\langle\hat{O}(t)\rangle = \mathrm{Tr}_{\mathscr{S}}\left[\int\mathrm{d}F_{\mathscr{D}}^{\mathrm{or}}\int\mathrm{d}F_{\mathscr{A}}^{\mathrm{or}}\hat{O}\hat{\sigma}(F_{\mathscr{D}}^{\mathrm{or}}, F_{\mathscr{A}}^{\mathrm{or}}; t)\right]$.

The dynamics starts upon impulsive excitation of the $\mathscr{D}$ molecule with $\hat{\sigma}(F_{\mathscr{D}}^{\mathrm{or}}, F_{\mathscr{A}}^{\mathrm{or}}; t = 0) = \hat{\sigma} \otimes w(F_{\mathscr{D}}^{\mathrm{or}}, F_{\mathscr{A}}^{\mathrm{or}})$, where $\hat{\sigma}(t = 0) = |\Psi^{\star}\rangle\langle\Psi^{\star}|$, and $|\Psi^{\star}\rangle = \sum_{a=2}^{N}|\psi_a\rangle\langle\psi_a|\hat{\mu}_{\mathscr{D}}|\psi_1\rangle$.[18] The

magenta contour plot in Fig. 4a shows the starting solvent distribution, $w(F_{\mathscr{D}}^{\mathrm{or}}, F_{\mathscr{A}}^{\mathrm{or}}; t = 0) = \exp[-E_1(F_{\mathscr{D}}^{\mathrm{or}}, F_{\mathscr{A}}^{\mathrm{or}})/k_{\mathrm{B}}T]$, where $E_1(F_{\mathscr{D}}^{\mathrm{or}}, F_{\mathscr{A}}^{\mathrm{or}})$ is the $(F_{\mathscr{D}}^{\mathrm{or}}, F_{\mathscr{A}}^{\mathrm{or}})$-dependent ground state potential energy (see ESI†). The equation of motion for the RET density matrix is the two-molecules analogue of eqn (3) and is reported in the ESI.†

Fig. 4 summarizes the calculated dynamics for the RET-pair in chloroform. Panels (a) and (b) show the system energy $\langle\hat{H}^{\mathrm{RET}}\rangle$ vs. the expectation values of the solvent reaction fields and of the vibrational coordinates, respectively. These quantities are shown as a function of time in panels (c–g). Coherent oscillations of $\mathscr{D}$ are observed with frequency ~0.18 eV (panel h). The corresponding solvent coordinate $F_{\mathscr{D}}^{\mathrm{or}}$ is too slow to follow vibrational oscillations: the black trace in Fig. 4a and $\langle F_{\mathscr{D}}^{\mathrm{or}}\rangle$ in Fig. 4d do not show any remnant oscillation. Coherent oscillations disappear in ~500 fs, when the energy starts flowing to $\mathscr{A}$, well before the system reaches the equilibrium in the $\mathscr{D}^{\star}\mathscr{A}$ PES. The expectation value of the coordinate $\hat{Q}_{\mathscr{A}}$, after showing very weak initial oscillations (peaking at ~0.13 eV, panel i), slowly moves towards its equilibrium geometry together with the relevant solvent coordinate, $F_{\mathscr{A}}^{\mathrm{or}}$ (see Fig. 4e).

To address the role of solvent dynamics in RET, we select the longest living eigenstates of $\hat{H}^{\mathrm{RET}}$ as representative of states $\mathscr{D}^{\star}\mathscr{A}$ (eigenstate number 94) and $\mathscr{D}\mathscr{A}^{\star}$ (eigenstate 92). In Fig. 5, we show the corresponding populations calculated at $t = 4.5$ ps in liquid CHCl$_3$ ($\tau_1 = 2.8$ ps, panel (a)) and in the same solvent, but setting $\tau_1 \to \infty$ (panel (b)), as relevant to a glassy solvent or to a solid matrix with the same dielectric properties as CHCl$_3$. In liquid solvent, after 4.5 ps only a residual $\mathscr{D}^{\star}\mathscr{A}$ population is observed, the energy being almost completely transferred to $\mathscr{D}\mathscr{A}^{\star}$. In glassy CHCl$_3$, instead, at the same delay time the $\mathscr{D}^{\star}\mathscr{A}$ population is only depleted along special directions in the solvent distribution, corresponding to those solvent configurations for which the vibronic states associated with $\mathscr{D}^{\star}\mathscr{A}$ and $\mathscr{D}\mathscr{A}^{\star}$ are almost degenerate. Accordingly, the $\mathscr{D}\mathscr{A}^{\star}$ population only builds up along the same special directions and the overall RET process dramatically slows down, as it can also be appreciated in the videos available in the ESI.† In either liquid or glassy matrices, RET occurs first along the fastest channels where good alignment of the involved energy levels is achieved. In frozen matrices, once the population of these fastest channels is depleted, RET can only proceed along slower channels. On the opposite, in the liquid solvent the population in the fastest channels is continuously replenished by the solvent rearrangement, leading to an overall faster RET, as confirmed by the t-dependence of the $(F_{\mathscr{D}}^{\mathrm{or}}, F_{\mathscr{A}}^{\mathrm{or}})$-integrated populations of $\mathscr{D}^{\star}\mathscr{A}$ and $\mathscr{D}\mathscr{A}^{\star}$ in Fig. 5c. To further confirm the picture, Fig. 5d shows the time evolution of the expectation value of the operator $\hat{\mathscr{S}}_{\mathscr{A}^{\star}}$ that measures the global $\mathscr{A}^{\star}$ population (defined in the ESI†) calculated in liquid CHCl$_3$ and in its glassy counterpart (solid and dashed lines, respectively): in the early time (<500 fs), RET velocity is similar in the two systems, but as soon as the liquid solvent diffusion enters into play, RET is much favored in the liquid solvent.
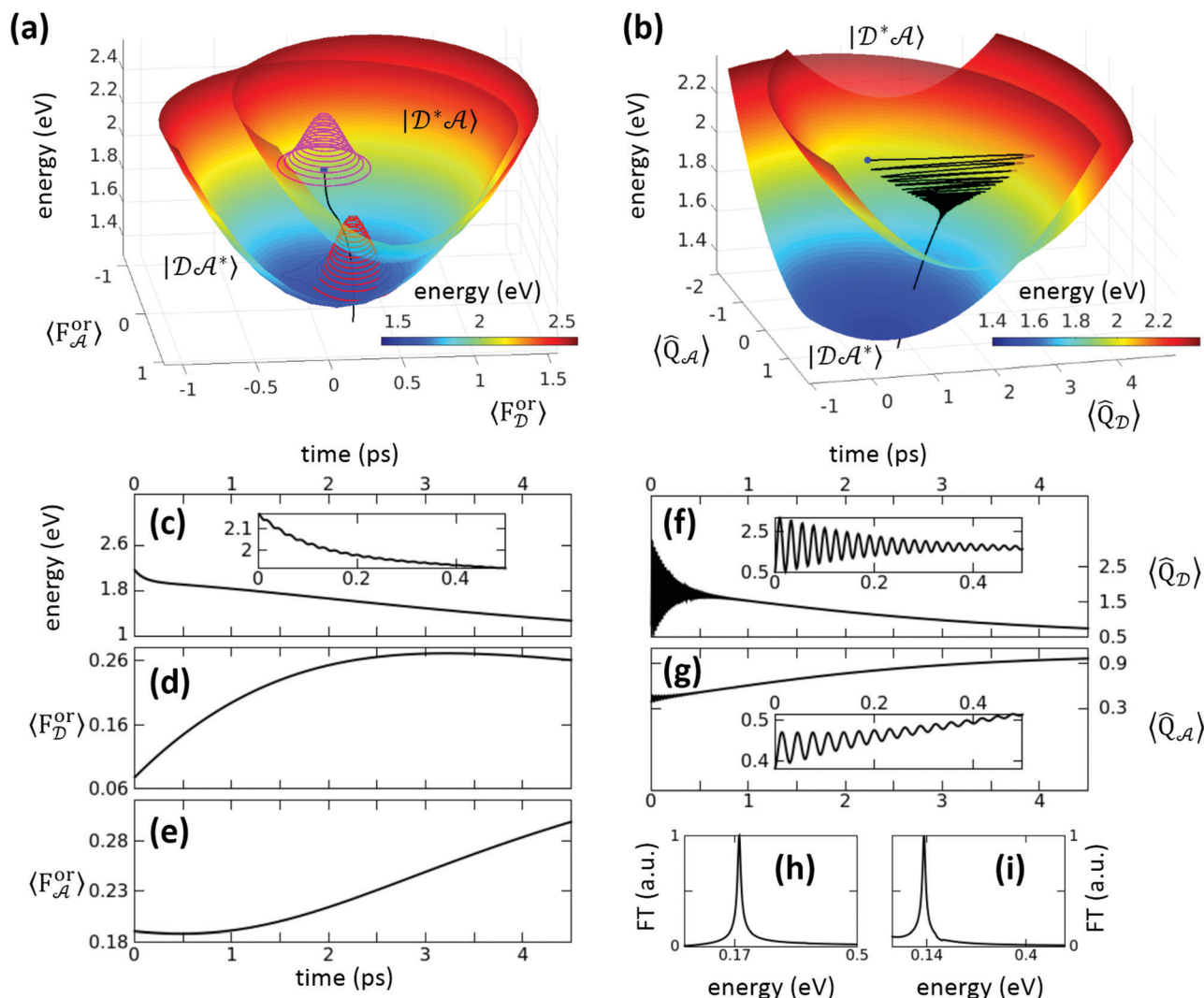
This journal is © the Owner Societies 2020

Phys. Chem. Chem. Phys., 2020, **22**, 1061–1068 | **1065**

Fig. 4 Room temperature dynamics calculated for the DCM–NR pair (molecular parameters in Table 1, $V = 0.01$ eV, $\gamma = 5$ ps^{-1}) dissolved in liquid CHCl$_3$ ($\tau_l = 2.8$ ps, $\varepsilon_{\mathscr{D}}^{or} = 0.32$ eV, $\varepsilon_{\mathscr{A}}^{or} = 0.47$ eV[25]). (a) The black trace shows the RET-pair energy *vs.* the expectation values of the polar solvation coordinates. The solvent distributions calculated at $t = 0$ and $t = 2.7$ ps are shown as three-dimensional contours in magenta and red, respectively. The adiabatic PES calculated for $Q_{\mathscr{D}} = 1.4$, $Q_{\mathscr{A}} = 1.3$ are shown for reference. (b) The black trace shows the RET-pair energy *vs.* the expectation values of the vibrational coordinates. The adiabatic PES calculated for $F_{\mathscr{D}}^{or} = 0.023$ eV, $F_{\mathscr{A}}^{or} = 0.027$ eV are shown for reference. In panels (a) and (b) a blue dot marks the trajectory starting point. (c) Time-evolution of the RET-pair energy. (d and e) Time-evolution of the solvation coordinates relevant to $\mathscr{D}$ and $\mathscr{A}$, respectively. (f and g) Time-evolution of $\mathscr{D}$ and $\mathscr{A}$ vibrational coordinates. (h) and (i) Fourier transforms of the signals in panels (f) and (g), respectively. Insets in panels (c), (f) and (g) zoom on the early-time dynamics.

6 Outlook

The proposed quantum-classical hybrid approach addresses the dynamics of a quantum system dissolved in a liquid polar solvent, accounting for the intertwined effects of non-adiabatic molecular vibrations and of solvent fluctuations. Fast processes, driven by the electronic polarization of the solvent, and slow processes, driven by polar solvation, are accounted for combining the Redfield theory with a multistate Smoluchowski equation. After validating the approach on steady-state and time-resolved spectra of a polar dye in solution, the fundamental problem of RET in a dynamically disordered medium is attacked, demonstrating that polar solvation dynamics, typically in the picoseconds time regime, boosts RET efficiency.

The molecular Hamiltonian in eqn (1) only describes a single effective molecular vibration that accounts for the overall electron-vibration coupling, in a similar spirit as the hierarchical representation in ref. 32 and 33. Of course more than a single mode must be accounted for if a precise description of vibrational spectra is needed,[34,35] with effects that are however marginal on electronic spectra. The presence of more than a single molecular mode would for sure open additional fast channels for RET in Fig. 5. However, since the electron-vibration coupling strength would be distributed among the modes, the overall RET velocity should only be marginally affected. For sure additional calculations on models with at least two explicit vibrations per molecule are in order to safely address this issue.
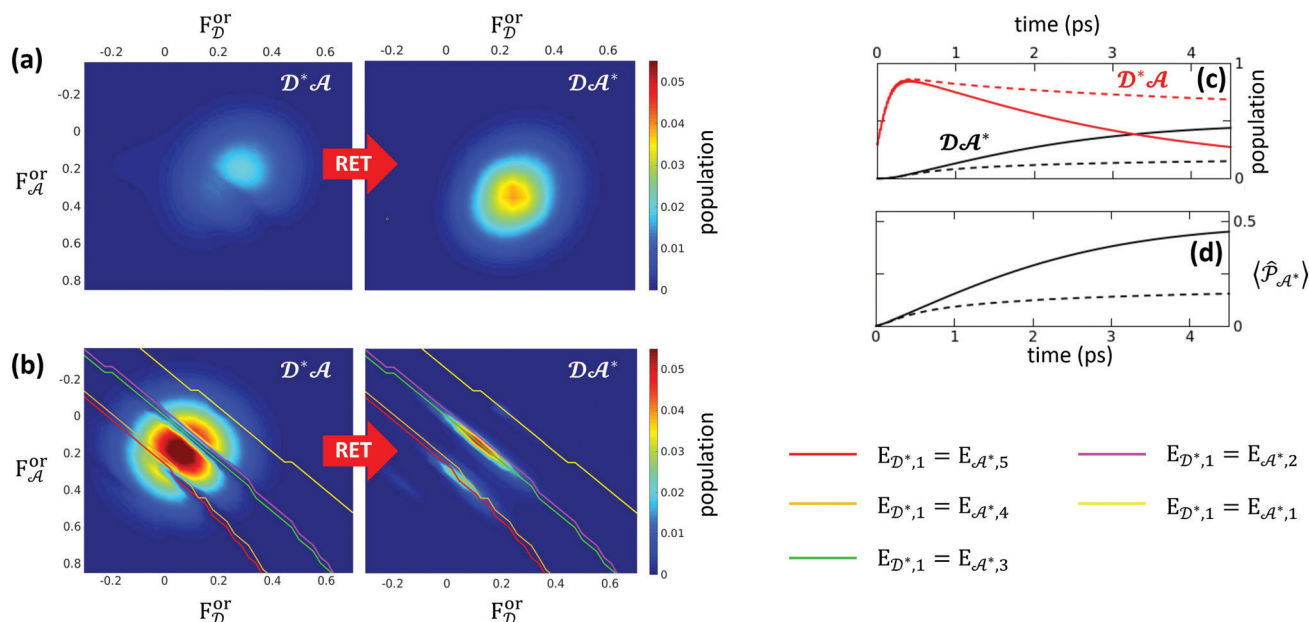
Fig. 5 (a) Two-dimensional maps calculated after a delay t = 4.5 ps in liquid CHCl$_3$ for the two representative states, $\sigma_{94,94}(F_{\mathscr{D}}^{or}, F_{\mathscr{A}}^{or})$ ($\mathscr{D}^*\mathscr{A}$) and $\sigma_{92,92}(F_{\mathscr{D}}^{or}, F_{\mathscr{A}}^{or})$ ($\mathscr{D}\mathscr{A}^*$), in the left and right panels, respectively. (b) The same quantities as in (a), but calculated at the same delay time in glassy CHCl$_3$. Colored lines correspond to solvent configurations for which the lowest excited state of the energy donor is degenerate with one of the first five lowest excited states of the energy acceptor. (c) Time-dependence of $\sigma_{94,94}$ (red curves) and $\sigma_{92,92}$ (black curves) as relevant to $\mathscr{D}^*\mathscr{A}$ and $\mathscr{D}\mathscr{A}^*$, respectively, for liquid (continuous curves) and glassy CHCl$_3$ (dashed curves); (d) time-dependent global population of $\mathscr{A}^*$ calculated in liquid (continuous curve) and glassy CHCl$_3$ (dashed curve). Same model parameters as in Fig. 4.

The novel Redfield–Smoluchowski equation (eqn (3)) offers a powerful strategy to address the effects of dynamical disorder on the dynamics of a photoexcited molecular system. It has been applied here to describe the effects of polar solvation on optical spectra of a polar dye as well as on RET dynamics. The same approach however can be adopted to describe other slow degrees of freedom affecting molecular properties, including *e.g.* conformational modes. The Redfield–Smoluchowski equation lends itself quite naturally to model symmetry-breaking in multipolar dyes,[36,37] the intertwined role of conformational motion and environmental degrees of freedom in thermally activated delayed fluorescence,[38] as well as the effect of dynamical disorder in exciton transport in molecular aggregates.[5]

Conflicts of interest

There are no conflicts to declare.

Acknowledgements

Notes and references

1   G. A. Jones and D. S. Bradshaw, *Front. Phys.*, 2019, **7**, 100.
2   T. Förster, *Ann. Phys.*, 1948, **437**, 55–75.
3   F. Levi, S. Mostarda, F. Rao and F. Mintert, *Rep. Prog. Phys.*, 2015, **78**, 082001.
4   C. Curutchet, B. Mennucci, G. D. Scholes and D. Beljonne, *J. Phys. Chem. B*, 2008, **112**, 3759–3766.
5   T. Mirkovic, E. E. Ostroumov, J. M. Anna, R. van Grondelle, R. Govindjee and G. D. Scholes, *Chem. Rev.*, 2017, **117**, 249–293.
6   A. Nazir, *Phys. Rev. Lett.*, 2009, **103**, 146404.
7   S. Athanasopoulos, E. V. Emelianova, A. B. Walker and D. Beljonne, *Phys. Rev. B: Condens. Matter Mater. Phys.*, 2009, **80**, 195209.
8   X. Chen and R. J. Silbey, *J. Phys. Chem. B*, 2011, **115**, 5499–5509.
9   T. Nelson, S. Fernandez-Alberti, A. E. Roitberg and S. Tretiak, *Phys. Chem. Chem. Phys.*, 2013, **15**, 9245–9256.
10 A. G. Redfield, *IBM J. Res. Dev.*, 1957, **1**, 19–31.
11 V. Chernyak and S. Mukamel, *J. Chem. Phys.*, 1996, **105**, 4565–4583.
12 A. Painelli, *Chem. Phys.*, 1999, **245**, 185–197.
13 F. Terenziani, A. Painelli and D. Comoretto, *J. Phys. Chem. A*, 2000, **104**, 11049–11054.
14 F. Terenziani and A. Painelli, *Chem. Phys.*, 2003, **295**, 35–46.
15 F. Terenziani and A. Painelli, *Phys. Chem. Chem. Phys.*, 2015, **17**, 13074–13081.
16 A. Painelli, *Chem. Phys. Lett.*, 1998, **285**, 352–358.
17 S. Sanyal, C. Sissa, F. Terenziani, S. K. Pati and A. Painelli, *Phys. Chem. Chem. Phys.*, 2017, **19**, 24979–24984.

This journal is © the Owner Societies 2020

Phys. Chem. Chem. Phys., 2020, **22**, 1061–1068 | **1067**

18 F. Di Maiolo and A. Painelli, *J. Chem. Theory Comput.*, 2018, **14**, 5339–5349.

19 J. Roden, W. T. Strunz, K. B. Whaley and A. Eisfeld, *J. Chem. Phys.*, 2012, **137**, 204110.

20 G. M. Beck and A. Sergi, *Phys. Lett. A*, 2013, **377**, 1047–1051.

21 G. M. Beck and A. Sergi, *J. Phys. A: Math. Theor.*, 2013, **46**, 395305.

22 A. Kelly, R. van Zon, J. Schofield and R. Kapral, *J. Chem. Phys.*, 2012, **136**, 084101.

23 S. Mukamel, *Principles of nonlinear optical spectroscopy*, Oxford University Press, 1995, pp. 358–359.

24 M. L. Horng, J. A. Gardecki, A. Papazyan and M. Maroncelli, *J. Phys. Chem.*, 1995, **99**, 17311–17337.

25 B. Boldrini, E. Cavalli, A. Painelli and F. Terenziani, *J. Phys. Chem. A*, 2002, **106**, 6286–6294.

26 M. L. Horng, J. A. Gardecki, A. Papazyan and M. Maroncelli, *J. Phys. Chem.*, 1995, **99**, 17311–17337.

27 Y. J. Yan and S. Mukamel, *J. Chem. Phys.*, 1988, **88**, 5735–5748.

28 T. Gustavsson, G. Baldacchino, J.-C. Mialocq and S. Pommeret, *Chem. Phys. Lett.*, 1995, **236**, 587–594.

29 P. van der Meulen, H. Zhang, A. M. Jonkman and M. Glasbeek, *J. Phys. Chem.*, 1996, **100**, 5367–5373.

30 C. Sissa, A. Painelli, M. Blanchard-Desce and F. Terenziani, *J. Phys. Chem. B*, 2011, **115**, 7009–7020.

31 C. Sissa, A. K. Manna, F. Terenziani, A. Painelli and S. K. Pati, *Phys. Chem. Chem. Phys.*, 2011, **13**, 12734–12744.

32 K. H. Hughes, C. D. Christ and I. Burghardt, *J. Chem. Phys.*, 2009, **131**, 124108.

33 I. Burghardt, R. Martinazzo and K. H. Hughes, *J. Chem. Phys.*, 2012, **137**, 144107.

34 A. Painelli and F. Terenziani, *Synth. Met.*, 2001, **116**, 135–138.

35 A. Girlando, M. Masino, A. Painelli, N. Drichko, M. Dressel, A. Brillante, R. G. Della Valle and E. Venuti, *Phys. Rev. B: Condens. Matter Mater. Phys.*, 2008, **78**, 045103.

36 F. Terenziani, A. Painelli, C. Katan, M. Charlot and M. Blanchard-Desce, *J. Am. Chem. Soc.*, 2006, **128**, 15742–15755.

37 F. Terenziani, C. Sissa and A. Painelli, *J. Phys. Chem. B*, 2008, **112**, 5079–5087.

38 F. B. Dias, T. J. Penfold and A. P. Monkman, *Methods Appl. Fluoresc.*, 2017, **5**, 012001.